

# Natural Band Alignments and Band Offsets of $\text{Sb}_2\text{Se}_3$ Solar Cells

Huw Shiel,<sup>†</sup> Oliver S. Hutter,<sup>†,¶</sup> Laurie J. Phillips,<sup>†</sup> Jack E. N. Swallow,<sup>†</sup>  
Leanne A. H. Jones,<sup>†</sup> Thomas J. Featherstone,<sup>†</sup> Matthew J. Smiles,<sup>†</sup>  
Pardeep K. Thakur,<sup>‡</sup> Tien-Lin Lee,<sup>‡</sup> Vinod R. Dhanak,<sup>†</sup> Jonathan D. Major,<sup>†</sup>  
and Tim D. Veal<sup>\*,†</sup>

<sup>†</sup>*Stephenson Institute for Renewable Energy and Department of Physics, University of  
Liverpool, Liverpool, L69 7ZF, United Kingdom*

<sup>‡</sup>*Diamond Light Source, Harwell Science & Innovation Campus, Didcot, OX11 0DE,  
United Kingdom*

<sup>¶</sup>*Department of Mathematics, Physics and Electrical Engineering, Northumbria University,  
Newcastle upon Tyne NE1 8ST, United Kingdom*

E-mail: T.Veal@liverpool.ac.uk

## Abstract

$\text{Sb}_2\text{Se}_3$  is a promising material for use in photovoltaics but the optimum device structure has not yet been identified. This study provides band alignment measurements between  $\text{Sb}_2\text{Se}_3$ , identical to that used in high efficiency photovoltaic devices, and its two most commonly used window layers, namely CdS and  $\text{TiO}_2$ . Band alignments are measured via two different approaches: Anderson's rule was used to predict an interface band alignment from measured natural band alignments, and the Kraut method was used in conjunction with hard x-ray photoemission spectroscopy to directly measure the band offsets at the interface. This allows examination of the effect of interface formation on the band alignments. The conduction band minimum (CBM) of  $\text{TiO}_2$  is found by the Kraut method to lie 0.82 eV below that of  $\text{Sb}_2\text{Se}_3$ , whereas the CdS CBM is only 0.01 eV below that of  $\text{Sb}_2\text{Se}_3$ . Furthermore, a significant difference is observed between the natural alignment- and Kraut method-determined offsets for  $\text{TiO}_2/\text{Sb}_2\text{Se}_3$ , whereas there is little difference for  $\text{CdS}/\text{Sb}_2\text{Se}_3$ . Finally, these results are related to device performance, taking into consideration how these results may guide the future development of  $\text{Sb}_2\text{Se}_3$  solar cells and providing a methodology which can be used to assess band alignments in device-relevant systems.

## Keywords

$\text{Sb}_2\text{Se}_3$ , Band Alignments, Window Layer, Photovoltaics, Photoemission, HAXPES

# Introduction

The field of solar energy has made great leaps forwards in recent years, leading the charge for a switch from the unsustainable burning of fossil fuels to a green energy future. While technologies such as crystalline silicon and cadmium telluride (CdTe) thin films have achieved great success industrially, there is a need for additional technologies when striving to achieve terawatt scale. Antimony selenide ( $\text{Sb}_2\text{Se}_3$ ) has all the desirable characteristics to be successful on an industrial level; it is a stable, binary compound made up of cheap and earth-abundant elements, it has a direct band gap of  $1.18 \text{ eV}^1$  and a very high absorption coefficient,  $>10^5 \text{ cm}^{-1}$ .<sup>2</sup> Its unusual 1D nanoribbon structure allows for very effective carrier transport if the correct orientation is achieved and has also been suggested to allow the formation of benign grain boundaries.<sup>3-5</sup> Furthermore the device performance has progressed rapidly since first being used in a solar cell,<sup>6,7</sup> reaching nearly 10% in 2019.<sup>8,9</sup>

These qualities make  $\text{Sb}_2\text{Se}_3$  a very promising material. However,  $\text{Sb}_2\text{Se}_3$  photovoltaics (PV) remains an emerging technology, with a significant amount of fundamental understanding still missing from the literature. The impact of this is felt particularly in the design of various device structures utilising different window layers (Figure 1). Cadmium sulfide (CdS) and titanium dioxide ( $\text{TiO}_2$ ) are both used frequently, with some studies finding CdS to offer superior performance<sup>3,10,11</sup> and others finding the switch to  $\text{TiO}_2$  extremely beneficial.<sup>4,12</sup> There are many aspects of these alternative device structures that are not understood, particularly the role of band alignments in influencing the device performance.

Band alignment is a general term used to describe the way the valence and conduction bands of two materials line up to perform a certain function. The ‘natural’ band alignment of two materials describes the positions of the band extrema with respect to the vacuum level when not in contact with each other. The term band offset refers to the separation of the band extrema between the two materials once contacted. A ‘spike-like’ band offset

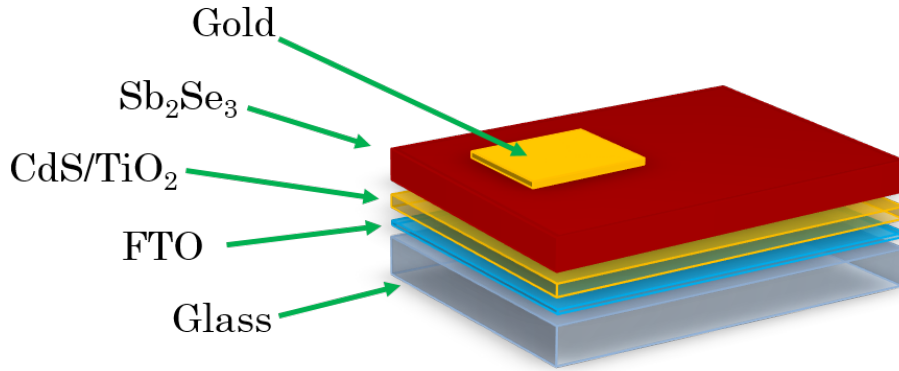


Figure 1: Schematic of the typical superstrate device structure used in  $\text{Sb}_2\text{Se}_3$  solar cells.

is defined as where the conduction band minimum (CBM) of the window layer lies above the CBM of the absorber, and a ‘cliff-like’ offset as when the CBM of the window layer lies below that of the absorber. Too positive an offset (Figure 2a), and electrons excited in the absorber will face a potential barrier opposing their drift into the window layer and lowering the short-circuit current ( $J_{sc}$ ) (and efficiency) of the cell. Too negative a CBO (Figure 2b) leads to a potential source of back-transfer carrier recombination at the interface between conduction band of the window layer and the valence band of the absorber. This recombination, in which electrons in the window layer recombine with holes in the absorber via interface states, is more likely the narrower the gap between the two energy levels<sup>13</sup>. A cliff-like offset also limits the built-in voltage ( $V_{bi}$ ) of the junction, leading to a lower open circuit voltage ( $V_{oc}$ ). The  $J_{sc}$  and  $V_{oc}$  are crucial aspects of the solar cell performance, therefore it is vital that a good band alignment is obtained for a PV technology to be successful.<sup>14,15</sup>

One of the best ways to measure band alignments is through photoemission techniques such as x-ray photoemission spectroscopy (XPS). Through use of the valence band and secondary electron cut-offs in an XPS spectrum, the ionisation potential and work function of a material can be measured relative to the vacuum level.<sup>16,17</sup> These quantities do not describe the interface itself, but via a method called Anderson’s rule the band alignment can be predicted. Another technique often employed is the Kraut method,<sup>18,19</sup> which allows the direct

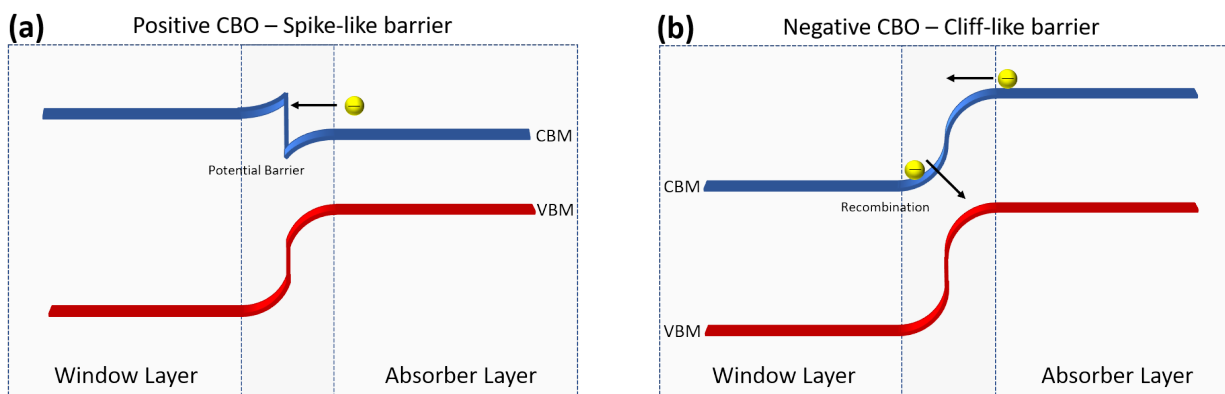


Figure 2: Schematic diagram showing (a) a very positive CBO leading to a potential barrier in the conduction band and (b) a very negative CBO leading to a recombination centre and low built-in voltage.

measurement of valence band offset (VBO) between two materials. Both methods employ a number of assumptions that will be discussed below.

In this study, the powerful photoemission techniques of traditional lab-based XPS and synchrotron-based hard x-ray photoemission spectroscopy (HAXPES) were used to measure and compare band alignments using both Anderson’s rule<sup>20</sup> and the Kraut method.<sup>18</sup> By examining the differences between the two sets of results, conclusions can be drawn about the effect of interface formation on the two different band alignments. Furthermore, by comparing these results to previous device studies, we assess the influence and impact of the band alignments on device performance characteristics.

## Methods

### Film Deposition

CdS films were deposited onto TEC10 fluorine-doped tin oxide (FTO) coated glass substrates (supplied by NSG Group) by RF-magnetron sputtering at 60 W, 5 mTorr of Ar gas and a substrate temperature of 200°C for 24 minutes. The CdS films were ~80 nm thick as

determined by an Ambios xp200 profilometer. Anatase TiO<sub>2</sub> films were deposited by a two step process; first an RF-magnetron sputtered film was deposited at room temperature at 150 W and 5 mTorr for 30 minutes, and secondly an established spin casting process<sup>21</sup> was carried out for a total film thickness of ~60 nm.

Sb<sub>2</sub>Se<sub>3</sub> films were deposited by close-space sublimation (CSS) at a source temperature of 390°C with substrate heating at 330°C and a base pressure of ~0.05 Torr. Interfacial films for band alignment measurements were deposited for only 30 seconds in order to achieve a film thin enough to carry out the Kraut method (~20 nm). For the ‘bulk’ samples, a thicker layer (~50 nm) was deposited so that the signal from the layer beneath was not seen in the HAXPES measurements. Detailed structural characterisation (including cross sectional transmission electron microscopy and x-ray diffraction) of similar films can be found in the work by Williams et al.<sup>5</sup>

## Photoemission

HAXPES measurements were carried out at the I09 beamline at Diamond Light Source, Oxfordshire, UK. A double-crystal Si(111) monochromator was used to select 5921 eV x-rays followed by a Si(004) channel-cut crystal resulting in energy resolution of 0.25 eV (as determined by measuring the Fermi edge of a polycrystalline gold reference sample at room temperature and fitting a Gaussian-broadened Fermi-Dirac distribution to the data). This allowed binding energy determination with a precision better than ±0.1 eV. The spectra were acquired using a Scienta Omicron EW4000 high-energy analyser with an acceptance angle of ±28°.

Lab-based XPS data was collected using a monochromated Al K $\alpha$  x-ray source ( $h\nu = 1486.6$  eV) operating at 250 W and a PSP Vacuum Systems hemispherical electron energy analyser with an acceptance angle of ±3° operating with a constant pass energy of 10 eV.

The energy resolution was determined to be 0.4 eV from fitting a Gaussian-broadened Fermi-Dirac distribution to the Fermi edge of a polycrystalline silver reference sample,<sup>22</sup> allowing binding energy determination with a precision of  $\pm 0.1$  eV.

All samples exhibited a small C 1s contaminant peak (and O 1s for the CdS sample) due to exposure to atmospheric conditions. The films were sufficiently conducting and were grounded to the spectrometer using a top electrical contact to avoid any surface charging effects.

## Measuring band alignments by photoemission

The measurement of the natural band alignments via photoemission is a commonly used procedure when screening materials for use as a junction partner to an absorber in a PV device.<sup>23,24</sup> While most studies use ultraviolet photoemission spectroscopy (UPS), a highly surface sensitive technique for studying work functions, it is also possible to use XPS which is slightly less surface sensitive (albeit still limited to the top few nanometres). This method involves measuring the ionisation potential of a material, which describes the position of the valence band maximum relative to the vacuum level, and then using either a measured or literature quoted band gap to determine the electron affinity, which describes the position of the conduction band relative to the vacuum level. When measuring ionisation potential, taking advantage of the fact that all XPS spectra are referenced to the Fermi level, the position of the Fermi level in the band gap can also be determined. Knowing that when two semiconductors are contacted the Fermi levels of the two must be aligned, there is a need for a model of how this affects the alignments of the conduction and valence bands at the interface.

## Anderson's Rule

One widely used approach is known as Anderson's rule or the electron affinity rule.<sup>20,23</sup> This method states that the Fermi levels of the two materials align, while maintaining the difference in natural electron affinity at the interface (Figure 3). However, this method does not take into account the role of charge transfer, orientation or interface induced gap states upon contacting two materials. Therefore, if the two materials have significantly different electronegativities or lattice spacing, this approximation could differ significantly from the real band alignment. <sup>23,25,26</sup> It also relies either on some assumptions, or complex additional measurements to determine how the band bending is distributed across the two sides of the interface.

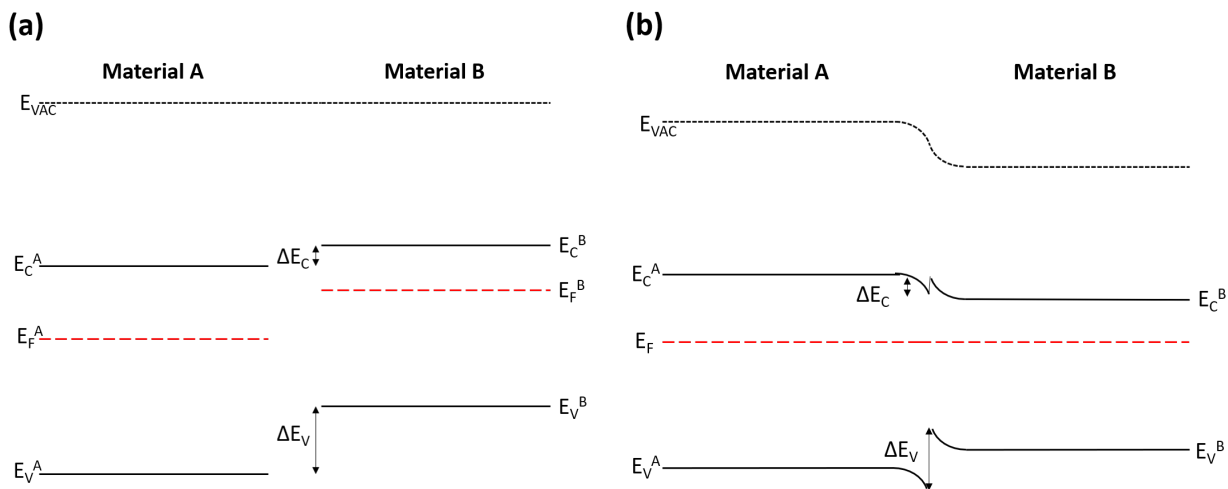


Figure 3: Schematic diagram of how band alignments are predicted using the Anderson rule with (a) showing the natural alignments referenced to the vacuum level and (b) showing band alignment after aligning Fermi levels.

## The Kraut Method

The alternative method used in this study, the Kraut method,<sup>18</sup> uses a combination of measurements to take into account the charge transfer across the interface between two



materials. First, the binding energy of high intensity core ( $E_{CL}$ ) levels and the VBM ( $E_V$ ) are measured for both materials in vacuum. Then a film of one material is deposited onto the other, thin enough that photoelectrons from the lower layer can still escape and be detected during an XPS measurement. This allows an interface-sensitive measurement in which peaks from both materials are resolved. Then by measuring the separation between core levels in the two materials ( $\Delta E_{CL}$ ) and exploiting the fact that the core level shift upon interface formation is equal to the shift in the valence and conduction bands ( $|\delta E_{CL}| = |\delta E_V| = |\delta E_C|$ ), the valence band offset between them can be directly determined, as shown in Figure 4 and equations 1:

$$\Delta E_V = (E_{CL}^B - E_V^B) - (E_{CL}^A - E_V^A) + \Delta E_{CL} \quad (1)$$

where  $A$  and  $B$  denote material  $A$  and material  $B$  and  $\Delta E_{CL} = E_{CL}^A - E_{CL}^B$ . They key difference between the Kraut method and Anderson's rule, therefore, is that Anderson's rule is a prediction of the band alignment based on measurements of the separate materials, whereas the Kraut method is a direct measurement of the band offset albeit with some simplifications. The Kraut method approach is an abrupt interface approximation, meaning that a single measurement gives only a single offset between the bands and, though the effects of band bending are accounted for, the band bending itself is not measured. Multiple measurements carried out during interface formation can provide more detailed measurements of the band bending, however this requires simultaneous in situ deposition and photoemission measurements, something that is not possible while using deposition techniques such as CSS. A drawback to this method, however, is sample preparation. As shown in Figure 5, the inelastic mean free path (IMFP) of a photoelectron is dependent on its kinetic energy and, according to the Beer-Lambert law, 95% of the signal originates within three IMFPs of the surface. Accordingly, the sampling depth of XPS is then roughly 10 nm, and a film thinner than this is required to carry out any Kraut method studies using conventional lab-based XPS.

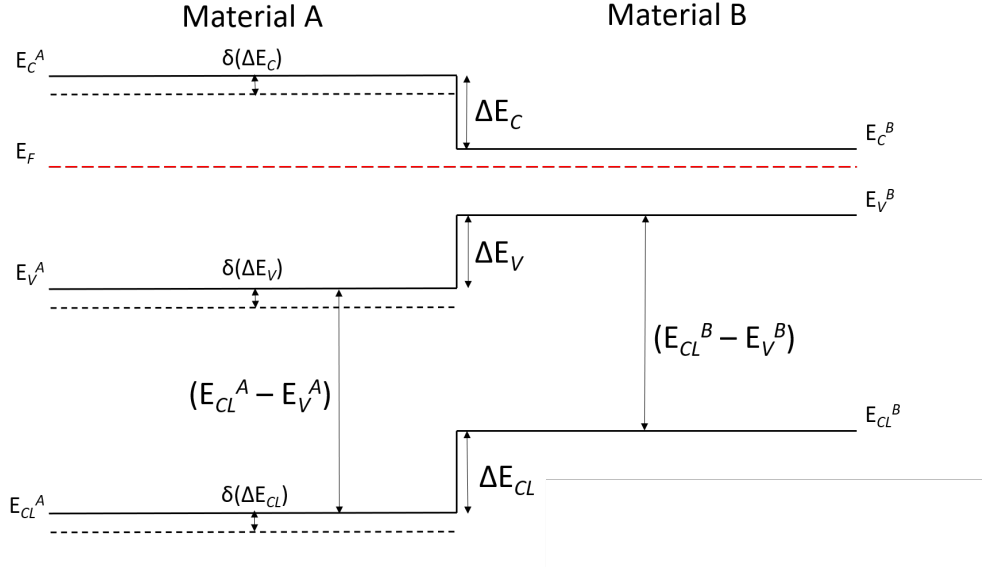


Figure 4: Schematic showing the band alignments measured by the Kraut method where  $\delta$  signifies the band energy shift due to interface formation and  $\Delta E$  signifies the band offsets.

Many of the recent advances in  $\text{Sb}_2\text{Se}_3$  device performance have come via the use of close space sublimation (CSS) or vapour transport deposition (VTD) of  $\text{Sb}_2\text{Se}_3$ .<sup>4,12,27,28</sup> CSS allows for the formation of large grain sizes with good preferred orientation for carrier transport. This does, however, limit the thickness of films that can be deposited while still achieving good coverage, which is essential to the validity of the Kraut method measurements. At roughly 20 nm, good coverage is achievable by CSS and this falls well within the sampling depth (Figure 5) of HAXPES, a synchrotron based technique that works by the same principle as conventional photoemission methods but with hard x-rays. With an excitation energy of 6000 eV, for example, the IMFP and effective probing depth of photoelectrons are greater than 9 nm and 27 nm respectively, for  $\text{Sb}_2\text{Se}_3$  (as calculated using the TPP-2M equation<sup>29</sup>). Using this method then, the band offset between a device-relevant layer of  $\text{Sb}_2\text{Se}_3$  and a window layer can be directly measured. Combining this with natural alignments measurements can provide powerful insights into the formation of these interfaces simply by observing the differences between the two measurements.

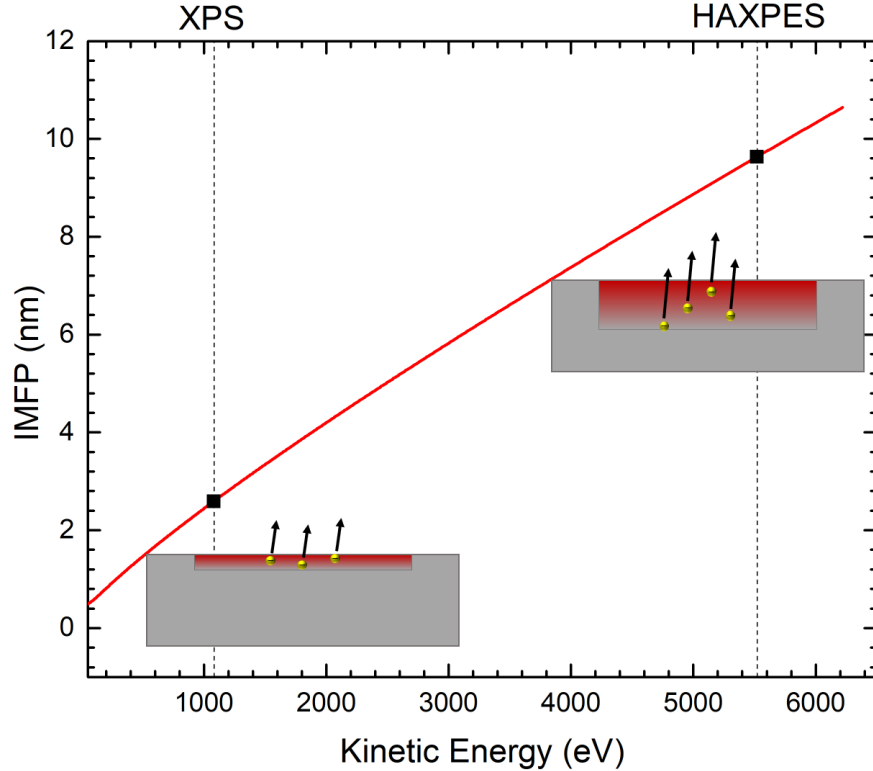


Figure 5: The inelastic mean free path of photoelectrons in  $\text{Sb}_2\text{Se}_3$  with respect to kinetic energy.<sup>29</sup> Black points show the kinetic energy of an electron escaping the Sb 3d orbital for both conventional Al  $K\alpha$  XPS (1486.6 eV) and HAXPES (assuming a photon energy of 5921 eV) and the inset sketches illustrate the relative probing depths of the two techniques.

Measurement of band alignments on material that was identical to that used in PV devices of good efficiency (>5%) was important to this study, because the properties of  $\text{Sb}_2\text{Se}_3$  are very sensitive to deposition method and material quality.<sup>4,12,30</sup> The following section includes results from natural band alignment measurements, Kraut method band offset measurements and a comparison to device performance characteristics. The films used for all three aspects of these results are directly comparable because they are all deposited from the same source material via the same deposition method. This is, to the best of our knowledge, the most device relevant measurement of band alignments in  $\text{Sb}_2\text{Se}_3$  solar cells performed to date. Through direct comparison of films and devices, this work provides a method by which improved window layer partners for  $\text{Sb}_2\text{Se}_3$  solar cells can be identified.

# Results

## Natural Alignments

Initially we measured the ionisation potential and work function of  $\text{Sb}_2\text{Se}_3$ ,  $\text{CdS}$  and  $\text{TiO}_2$  films that were deposited under the same conditions used for fabrication of devices.<sup>4,12</sup> Figure 6 shows the secondary electron cut-off and valence band edge of  $\text{TiO}_2$ ,  $\text{CdS}$  and  $\text{Sb}_2\text{Se}_3$  that are used to measure the valence band and Fermi level positions of each material with respect to the the vacuum level. Each cut-off was fitted with a linear fit. As can be seen in Figure 6, while the gradients naturally vary between the samples there are no unusual shapes to any of the cut-offs.

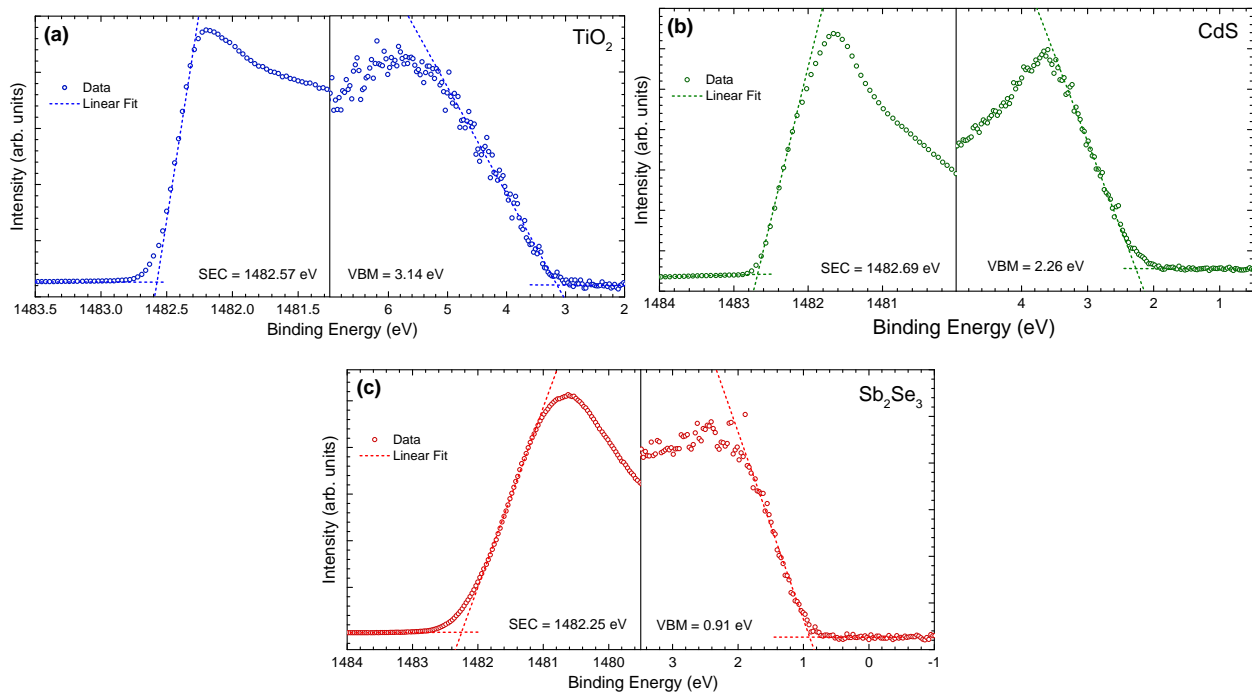


Figure 6: Secondary electron cut-off (SEC) and valence band maximum (VBM) obtained by XPS for ‘bulk’ samples of (a)  $\text{TiO}_2$ , (b)  $\text{CdS}$  and (c)  $\text{Sb}_2\text{Se}_3$  with linear fits.

Using the data from Figure 6 and literature band gap values,<sup>1,31–33</sup> the electron affinity of each material can be inferred and subsequently a band diagram drawn (Figure 7a). From Figure 7a it can be seen that all three materials are n-type. The n-type conductivity of

$\text{Sb}_2\text{Se}_3$  is a result of the presence of chlorine impurities in the purchased source material - a more detailed discussion of n-type  $\text{Sb}_2\text{Se}_3$  as well as the formation of an isotype heterojunction is provided by Hobson *et al.*<sup>34</sup>

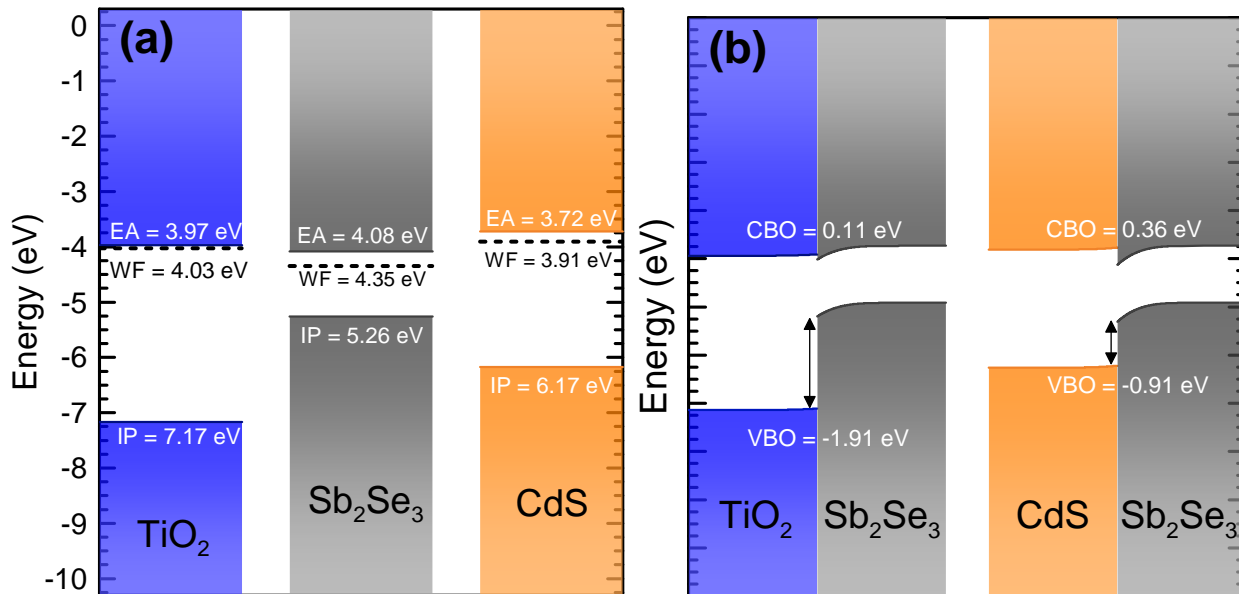


Figure 7: (a) Natural Alignments of  $\text{Sb}_2\text{Se}_3$  (grey) alongside  $\text{TiO}_2$  (blue) and  $\text{CdS}$  (orange) with the Fermi levels aligned. (b) Band alignments when the Fermi levels of the window layers are aligned with that of  $\text{Sb}_2\text{Se}_3$ . The band gaps used for  $\text{TiO}_2$ ,  $\text{Sb}_2\text{Se}_3$  and  $\text{CdS}$  were 3.2 eV, 1.18 eV and 2.45 eV respectively.

Figure 7b shows the alignment between  $\text{Sb}_2\text{Se}_3$  and  $\text{TiO}_2$  and between  $\text{Sb}_2\text{Se}_3$  and  $\text{CdS}$  if the Fermi levels are aligned according to Anderson's rule. According to this rule, the difference in electron affinity is fixed at the interface, leading to a small spike of 0.36 eV between  $\text{CdS}$  and  $\text{Sb}_2\text{Se}_3$  and a smaller spike of 0.11 eV between  $\text{TiO}_2$  and  $\text{Sb}_2\text{Se}_3$ . The bulk band positions of each material are determined from Figure 7a and are shifted up/down to align the Fermi levels. Band bending is then incorporated to resolve the discontinuity. An assumption has to be made regarding the distribution of the band bending - in this case it is almost entirely in the  $\text{Sb}_2\text{Se}_3$  given that the majority of the band bending will occur in the material with the lowest carrier density<sup>26</sup> and that  $\text{Sb}_2\text{Se}_3$  is known to undergo significant band bending at the surface.<sup>34</sup> From this it would appear that  $\text{Sb}_2\text{Se}_3$  and  $\text{CdS}$  have a good alignment for effective carrier transport in a PV device - a small spike up to 0.4

eV is widely considered to be conducive to achieving high efficiencies<sup>14,35,36</sup> by maximising available voltage and minimising the chance of recombination while maintaining a CBO small enough for carriers to overcome.

## Band Offset Measurements

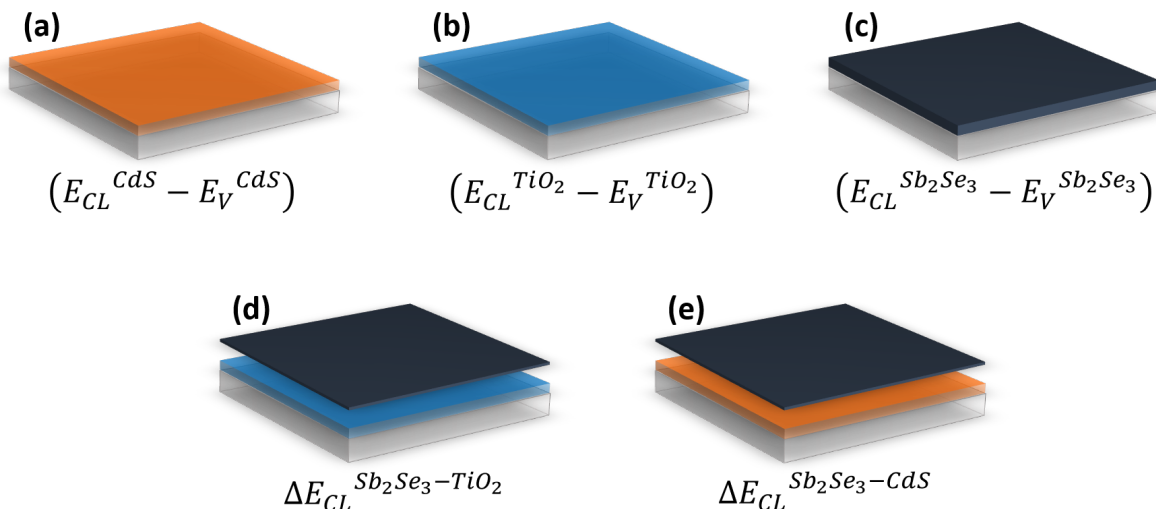


Figure 8: Sample set used for Kraut method band offset measurements along with quantities measured from each one: (a-c) show ‘bulk’ samples of (a) CdS, (b) TiO<sub>2</sub> and (c) Sb<sub>2</sub>Se<sub>3</sub>, and (d-e) show ‘interfacial’ samples of (d) Sb<sub>2</sub>Se<sub>3</sub> on TiO<sub>2</sub> and (e) Sb<sub>2</sub>Se<sub>3</sub> on CdS.

The Kraut method approach takes into account the charge transfer between the two materials by directly measuring the interface between them. In this study, HAXPES was used in order to enhance the inelastic mean free path of the photoemitted electrons, thereby allowing us to measure band alignments with a thicker layer of Sb<sub>2</sub>Se<sub>3</sub> (~20 nm). Figure 9 shows the photoemission data collected for the band alignment between Sb<sub>2</sub>Se<sub>3</sub> and either CdS or TiO<sub>2</sub> (sample set shown in Figure 8). Figures 9a-c show survey scans including insets of the detailed valence band scans used to determine VBM positions for each material. Figures 9d & 9e show survey scans of the interfacial samples with insets showing the separately measured core levels from the window layers. Core level and VBM binding energies are included in Table S1. Detailed scans of the Ti, Cd and the Sb core-levels used and the respective valence bands are included in Supporting Information (Figures S1-S5).

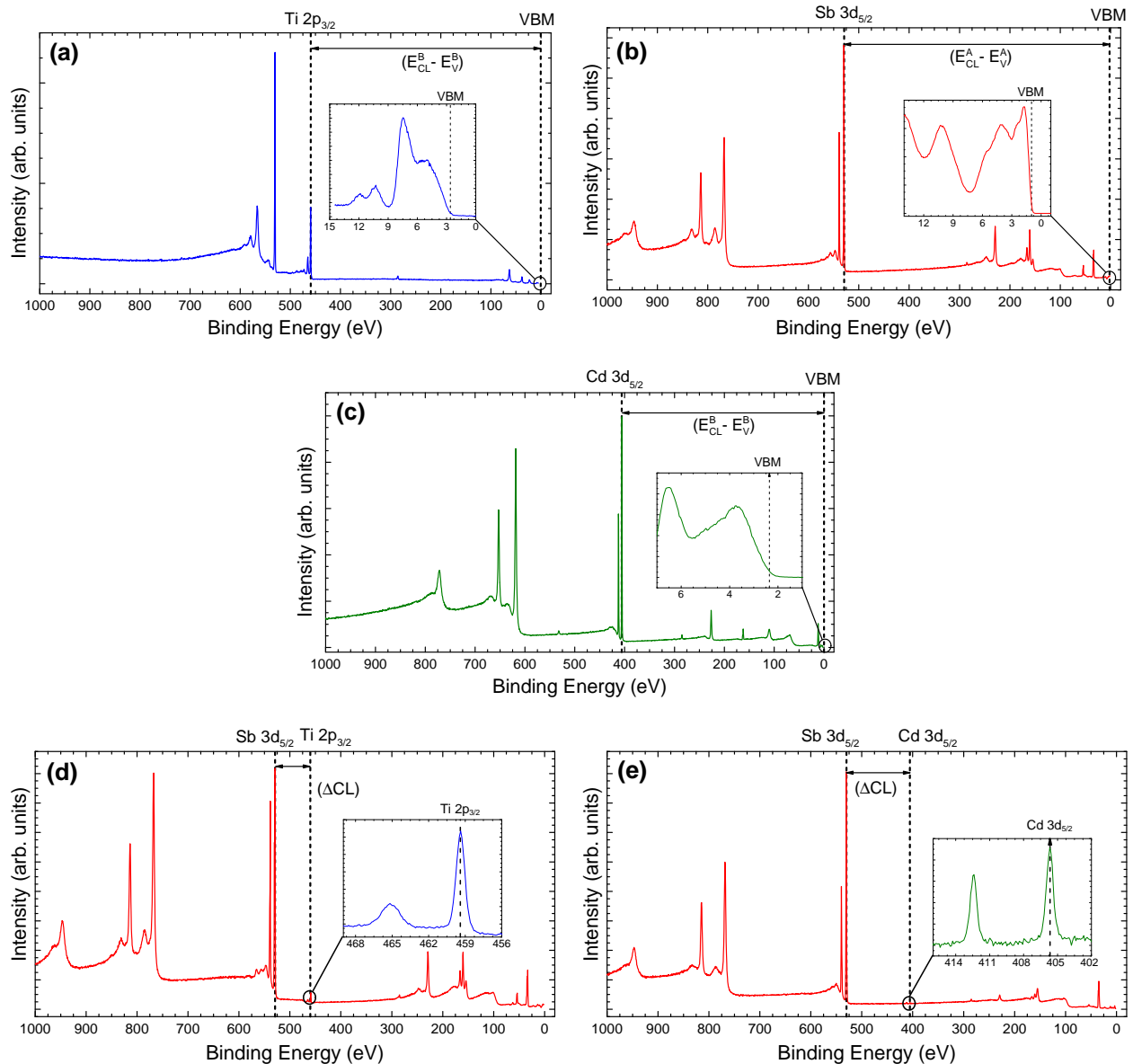


Figure 9: HAXPES data used to calculate band offsets. (a-c) show survey scans of ‘bulk’ (a) TiO<sub>2</sub>, (b) Sb<sub>2</sub>Se<sub>3</sub> and (c) CdS with separately measured VBMs shown in insets. (d-e) show the ‘interfacial’ samples of (d) Sb<sub>2</sub>Se<sub>3</sub> on TiO<sub>2</sub> and (e) Sb<sub>2</sub>Se<sub>3</sub> on CdS with the separately measured core level peaks from the substrates shown in the inset.

Figure 10a shows the band offsets drawn from the VBOs measured by the Kraut method using HAXPES of Sb<sub>2</sub>Se<sub>3</sub> on both CdS and TiO<sub>2</sub>. In the Kraut method approach, no bulk band positions are measured and the offsets acquired are representative of the interface only.

The VBOs were obtained using a number of characteristic  $\text{Sb}_2\text{Se}_3$  peaks (Sb 3d, Sb 4d and Se 3d) but only one window layer peak was used as only the most intense one was resolvable (Cd 3d & Ti 2p) due to the attenuation of the window layer photoelectrons by the  $\text{Sb}_2\text{Se}_3$  overlayer. The values presented in this work are an average of the VBOs calculated from the different core levels - the full breakdown of values is included in Table S2. The  $\text{Sb}_2\text{Se}_3/\text{CdS}$  interface has a small CBO of  $-0.01$  eV. The band alignment between  $\text{Sb}_2\text{Se}_3$  and  $\text{TiO}_2$  corresponds to a large cliff-like CBO of  $-0.82$  eV. These appear significantly different to the natural alignment results at first glance. However, before the two measurements can be compared, the impact of the assumptions and approximations involved in the two approaches must be considered.

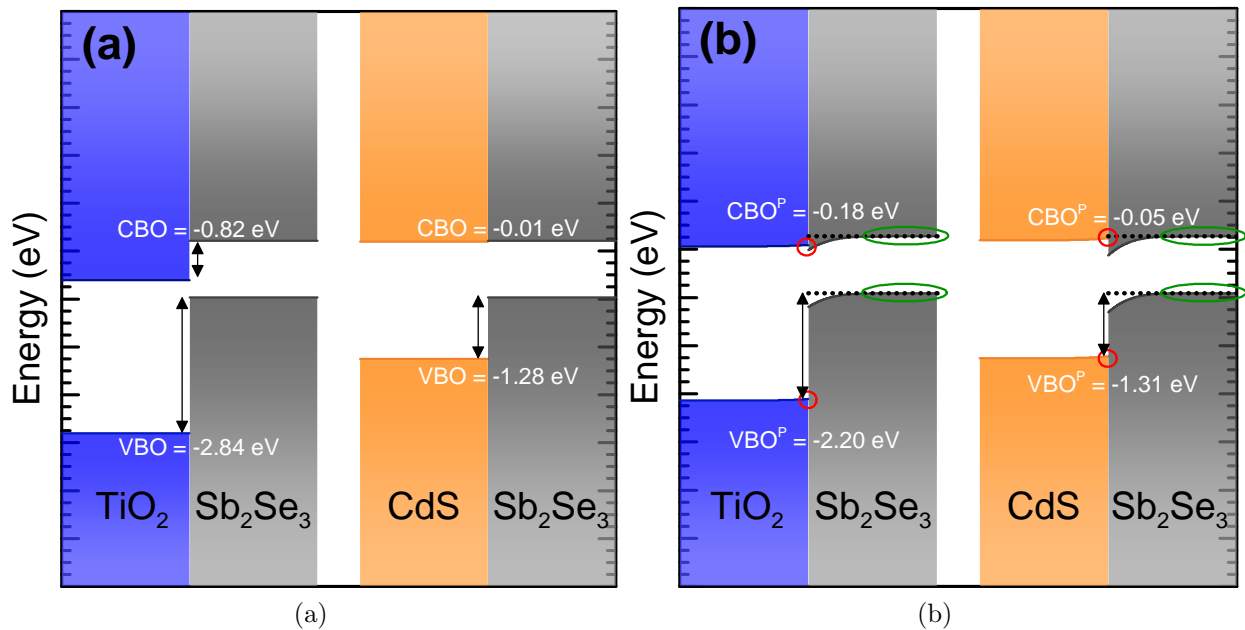


Figure 10: (a) Band offsets measured via the Kraut method using HAXPES and (b) natural alignments calculated by Anderson's rule (Figure 7b), with red and green circles indicating the equivalent regions probed by the Kraut method in window layer and  $\text{Sb}_2\text{Se}_3$  respectively.



# Discussion

The measurement of the band offsets via the Kraut method assumes flat bands and an abrupt junction. However, we must consider which regions of the interface contribute most strongly to the photoemission spectra. From the weakness of Ti 2p signal from the TiO<sub>2</sub> layer in Figure 9d (and similarly for Cd 3d from the CdS), it is clear that only a very thin part of the window layer would be detected, right at the interface with Sb<sub>2</sub>Se<sub>3</sub> (red circles in Figure 10b). For the Sb<sub>2</sub>Se<sub>3</sub>, we can be sure that the bulk band position (green circles in Figure 10b) will dominate the signal considering that, as shown in Figure 5, the Beer-Lambert law dictates that 63% of the signal will originate from the top 9 nm. This leads us to assume that the most relevant comparison between the natural alignments and the Kraut method is as depicted in Figure 10b. Figure 10b shows the same data as presented in Figure 7b, with coloured circles to indicate the equivalent regions that would be probed by the Kraut method. The predicted offsets (CBO<sup>P</sup> and VBO<sup>P</sup>) presented in Figure 10b show the energy separation between these circled regions of the Sb<sub>2</sub>Se<sub>3</sub> and respective window layers, for easy comparison with Figure 10a. Therefore the predicted band offsets quoted in Figure 10b are not measured, but are rather a projection of what the interface predicted by Anderson's rule (Figure 7b), in the absence of interface charge transfer, would yield if measured via the Kraut method.

Based on this assumption, comparing Figures 10a and 10b we can see that for the CdS/Sb<sub>2</sub>Se<sub>3</sub> interface there is very good agreement between the Kraut method and Anderson's rule. This strengthens the conclusion that CdS and Sb<sub>2</sub>Se<sub>3</sub> have excellent band alignments for good device performance in photovoltaics and suggests that the band alignment between CdS and Sb<sub>2</sub>Se<sub>3</sub> predicted by Anderson's rule is an accurate prediction of the true band alignment. However, for the TiO<sub>2</sub>/Sb<sub>2</sub>Se<sub>3</sub> interface, there is a significant difference between VBO and CBO given by the Kraut method and the modified Anderson's rule results. Even when taking into account the differences between the two approaches regarding

band bending (Figure 10b), the predicted offset (CBO<sup>P</sup>) between the flat band position in the Sb<sub>2</sub>Se<sub>3</sub> and the edge of the TiO<sub>2</sub> band is only -0.18 eV in the modified Anderson model, compared to a CBO of -0.82 eV measured by the Kraut method. According to the Kraut method here, even with an equivalent amount of band bending as predicted by Anderson's rule, the CBO would actually be cliff-like at the interface (Figure 10a), rather than the 0.11 eV spike predicted by Anderson's rule (Figure 7b). This suggests that there is a large degree of charge transfer upon contacting which increases the VBO (and CBO) from the natural value. The existence of a cliff-like offset is supported by the observation of a similar alignment for Sb<sub>2</sub>S<sub>3</sub> and TiO<sub>2</sub> reported elsewhere.<sup>37</sup>

There is a significant difference in how closely matched the natural alignment and Kraut method results are for Sb<sub>2</sub>Se<sub>3</sub>/CdS and Sb<sub>2</sub>Se<sub>3</sub>/TiO<sub>2</sub>. For the Sb<sub>2</sub>Se<sub>3</sub>/CdS interface, the difference is minimal. The similitude of sulphur and selenium as anions in terms of both valency and electronegativity could play a part in this. While the electronegativity of all three cations (Ti, Cd and Sb) are all reasonably similar (1.54, 1.69 and 2.05), the electronegativity of O (3.44) is far greater than those of S and Se (2.58 and 2.55), which are almost equal.<sup>38-40</sup> This means that CdS and Sb<sub>2</sub>Se<sub>3</sub> are expected to have a similar overall electronegativity, while the electronegativity of TiO<sub>2</sub> is expected to be significantly greater (there being twice as many O atoms as Ti). A smaller electronegativity difference between the two contacted materials means less charge transfer upon contacting and a smaller interface dipole.<sup>38,41</sup>

From a device performance perspective, the results of the band alignment measurements show that the CdS/Sb<sub>2</sub>Se<sub>3</sub> interface has a better alignment than TiO<sub>2</sub>/Sb<sub>2</sub>Se<sub>3</sub> - according to the Kraut method TiO<sub>2</sub> would form a large cliff-like barrier at the interface with Sb<sub>2</sub>Se<sub>3</sub>, leading to a limited available voltage from these kinds of devices. CdS, however, has a conduction band which is perfectly aligned with the conduction band of Sb<sub>2</sub>Se<sub>3</sub>, showing that this would provide a near-perfect window layer partner, at least in terms of band alignment

- a small interfacial spike between 0.3 eV and 0.4 eV has been shown to be ideal for PV devices with materials such as CZTS and CdTe.<sup>14,35,36</sup> Additionally, the difference between the natural alignment and Kraut method offsets presents some interesting insights into the formation of these interfaces.

Interestingly, however, CdS-based devices do not necessarily perform better than TiO<sub>2</sub>-based devices. It has been shown by our group previously that for Sb<sub>2</sub>Se<sub>3</sub> films grown by CSS, the devices utilising a CdS window layer perform very poorly compared to those using TiO<sub>2</sub>.<sup>12</sup> Phillips *et al.* reported a power conversion efficiency of only 1.44% for a CdS-based device compared to 5.48% for a TiO<sub>2</sub>-based device. While the  $V_{oc}$  and FF were somewhat lower for CdS (0.42 V & 45.48%) than for TiO<sub>2</sub> (0.45 V & 48.96%), the most significant difference was in the  $J_{sc}$ : only 7.57 mA.cm<sup>-2</sup> for CdS compared to 25.44 mA.cm<sup>-2</sup> for TiO<sub>2</sub>. This is the opposite of what would be expected from the band alignments measured in this study - the cliff-like offset of the TiO<sub>2</sub>/Sb<sub>2</sub>Se<sub>3</sub> interface would be expected to cause a lower  $V_{oc}$  than CdS/Sb<sub>2</sub>Se<sub>3</sub>, and the small CBO of the CdS/Sb<sub>2</sub>Se<sub>3</sub> lead to a very good current. This discrepancy is attributed to interdiffusion of the anions, S and Se, across the interface during the high temperature growth stage of the Sb<sub>2</sub>Se<sub>3</sub> devices, a process which leads to the formation of a CdSe layer in between the Sb<sub>2</sub>Se<sub>3</sub> and CdS.<sup>12</sup> This is evidenced by time-of-flight secondary ion mass spectrometry and external quantum efficiency measurements by Phillips *et al.*<sup>12</sup> and significantly reduces the efficiency of the carrier transport from absorber to window layer (the intermixing is not present in the samples used for the band alignments measurements as discussed below). This is further illustrated by Williams *et al.* where the overlapping presence of Cd, S and Se at the interface, as well as the possible presence of metallic Sb is shown with cross-sectional transmission electron microscopy with elemental mapping.<sup>5</sup> The implication of this is that it may be possible to achieve a superior device performance if the interdiffusion can be prevented in such a way that the favourable band alignment between CdS and Sb<sub>2</sub>Se<sub>3</sub> can be retained.

While the intermixed region is ever-present in the working devices, it is noted here that intermixing is not expected to occur in the samples presented here.  $\text{Sb}_2\text{Se}_3$  films deposited by CSS for devices are made via a two step process, an initial step at lower temperature to lay down a seed layer and then a longer, higher temperature deposition in order to achieve a good grain size/structure. Given that for the interfacial samples the deposition was only 30 seconds long and at the lower temperature used to deposit the seed layer, it is assumed that no significant intermixing was able to occur. Additionally, there is no evidence of any additional chemically shifted components in the photoemission spectra that could be attributed to CdSe or  $\text{Sb}_2\text{S}_3$  in the interface region.

It is noteworthy here that the current record efficiency for any  $\text{Sb}_2\text{Se}_3$  solar cell is held by Li *et al.*,<sup>8</sup> and that in their study a thin  $\text{TiO}_2$  interlayer deposited by atomic layer deposition was used between CdS and  $\text{Sb}_2\text{Se}_3$  to block a similar interdiffusion process. While it must be acknowledged that the devices made by Li *et al.* contained a number of differences from the standard  $\text{Sb}_2\text{Se}_3$  device structure considered in this work (the use of a substrate configuration and a nanorod structure among them), it is promising to the conclusions of this work that to the best of our knowledge the only study in which steps have been taken to prevent the interdiffusion between CdS and  $\text{Sb}_2\text{Se}_3$  has achieved such outstanding performance. We postulate, therefore, that the band alignments between  $\text{TiO}_2$  and  $\text{Sb}_2\text{Se}_3$  are a limit to the potential efficiency of  $\text{Sb}_2\text{Se}_3$  devices that use  $\text{TiO}_2$  as a window layer. Furthermore, by utilising CdS as a window layer (while blocking interdiffusion with an interlayer thin enough not to interfere significantly with the band alignments), the efficiencies of  $\text{Sb}_2\text{Se}_3$  solar cells could be improved beyond 10%.

## Conclusion

In this work we have used photoemission techniques to thoroughly study the band alignments between  $\text{Sb}_2\text{Se}_3$  and two of its most commonly used window layers - CdS and  $\text{TiO}_2$ . The result of natural alignment measurements showed CdS and  $\text{Sb}_2\text{Se}_3$  to have a small CBO of 0.36 eV while the offset between  $\text{Sb}_2\text{Se}_3$  and  $\text{TiO}_2$  CBO was 0.11 eV. Kraut method measurements carried out using HAXPES revealed a similar result for  $\text{Sb}_2\text{Se}_3/\text{CdS}$  of -0.01 eV while the offset for  $\text{Sb}_2\text{Se}_3/\text{TiO}_2$  was significantly different at -0.82 eV. The results suggest that CdS has an optimal band alignment with  $\text{Sb}_2\text{Se}_3$  while  $\text{TiO}_2$ -based devices are likely limited by a cliff-like offset leading to recombination and a limited built-in voltage. This is especially relevant considering the evidence of detrimental intermixing at CdS/ $\text{Sb}_2\text{Se}_3$  interfaces. This has led some groups to prefer the use of  $\text{TiO}_2$  as a window layer and has also inspired the use of an interdiffusion blocking interlayer in a recent record efficiency publication.<sup>8</sup> The harnessing of advantageous band alignments whilst preventing interdiffusion could provide a platform for pushing the efficiencies of  $\text{Sb}_2\text{Se}_3$  to the next level.

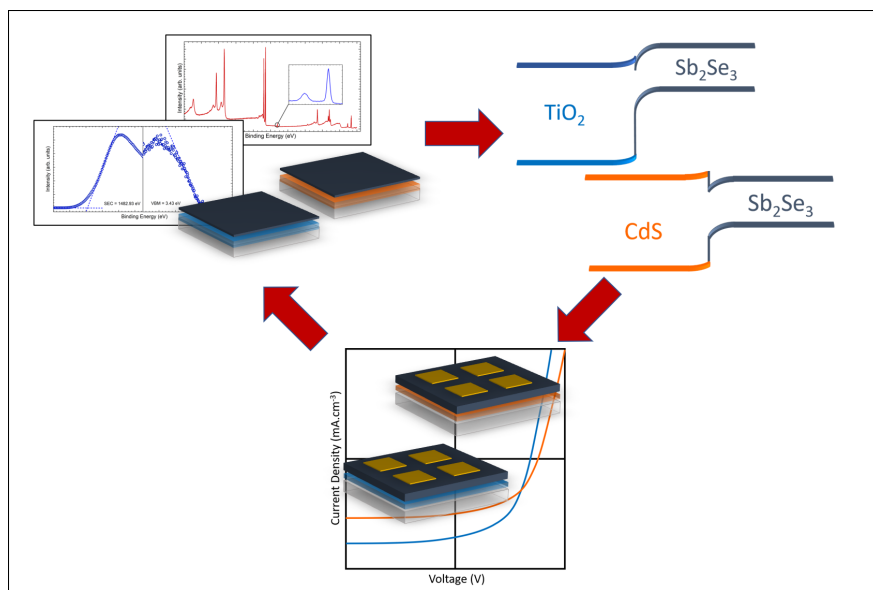
## Acknowledgements

The Engineering and Physical Sciences Research Council (EPSRC) is acknowledged for funding of H.S. (Grant No. EP/N509693/1), O.S.H. (Grant No. EP/M024768/1), L.A.H.J. (Grant No. EP/R513271/1), J.E.N.S., T.J.F., and M.J.S. (Grant No. EP/L01551X/1), L.J.P. and J.D.M. (Grant No. EP/N014057/1), and V.R.D. and T.D.V. (Grant No. EP/N015800/1). The XRD facility was supported by the EPSRC under Grant No. EP/P001513/1. Paul Warren of NSG Group is thanked for discussions, funding of H.S. and for supplying coated glass substrates. Diamond Light Source is acknowledged for I09 beam time under proposal SI23160-1.

## Supporting Information

Tables detailing binding energy of all fitted core levels and valence bands and the calculated band offsets. Graphs showing core level and band edge fits for all photoemission results.

### For Table of Contents Only



## References

- (1) Birkett, M.; Linhart, W. M.; Stoner, J.; Phillips, L. J.; Durose, K.; Alaria, J.; Major, J. D.; Kudrawiec, R.; Veal, T. D. Band gap temperature-dependence of close-space sublimation grown  $\text{Sb}_2\text{Se}_3$  by photo-reflectance. *APL Materials* **2018**, *6*, 084901.
- (2) Chen, C.; Li, W.; Zhou, Y.; Chen, C.; Luo, M.; Liu, X.; Zeng, K.; Yang, B.; Zhang, C.; Han, J.; Tang, J. Optical properties of amorphous and polycrystalline  $\text{Sb}_2\text{Se}_3$  thin films prepared by thermal evaporation. *Applied Physics Letters* **2015**, *107*, 043905.
- (3) Zhou, Y.; Wang, L.; Chen, S.; Qin, S.; Liu, X.; Chen, J.; Xue, D. J.; Luo, M.; Cao, Y.; Cheng, Y.; Sargent, E. H.; Tang, J. Thin-film  $\text{Sb}_2\text{Se}_3$  photovoltaics with oriented one-dimensional ribbons and benign grain boundaries. *Nature Photonics* **2015**, *9*, 409–415.
- (4) Hutter, O. S.; Phillips, L. J.; Durose, K.; Major, J. 6.6% efficient antimony selenide solar cells using grain structure control and an organic contact layer. *Solar Energy Materials Solar Cells* **2018**, *188*, 177 – 181.
- (5) Williams, R. E.; Ramasse, Q. M.; McKenna, K. P.; Phillips, L. J.; Yates, P. J.; Hutter, O. S.; Durose, K.; Major, J. D.; Mendis, B. G. Evidence for Self-healing Benign Grain Boundaries and a Highly Defective  $\text{Sb}_2\text{Se}_3$ –CdS Interfacial Layer in  $\text{Sb}_2\text{Se}_3$  Thin-Film Photovoltaics. *ACS Applied Materials & Interfaces* **2020**, *12*, 21730–21738.
- (6) Luo, M.; Leng, M.; Liu, X.; Chen, J.; Chen, C.; Qin, S.; Tang, J. Thermal evaporation and characterization of superstrate  $\text{CdS}/\text{Sb}_2\text{Se}_3$  solar cells. *Applied Physics Letters* **2014**, *104*, 173904.
- (7) Liu, X. and Chen, J. and Luo, M. and Leng, M. and Xia, Z. and Qin, S. and Xue, D-J. and Lv, L. and Huang, H. and Niu, D. and Tang, J., Thermal evaporation and characterization of  $\text{Sb}_2\text{Se}_3$  thin film for substrate  $\text{Sb}_2\text{Se}_3/\text{CdS}$  solar cells. *ACS Applied Materials & Interfaces* **2014**, *6*, 10687–10695.

- (8) Li, Z.; Liang, X.; Li, G.; Liu, H.; Zhang, H.; Guo, J.; Chen, J.; Shen, K.; San, X.; Yu, W.; Schropp, R. E. I.; Mai, Y. 9.2%-Efficient Core-Shell Structured Antimony Selenide Nanorod Array Solar Cells. Nature Communications **2019**, 10, 1–9.
- (9) Wong, L. H.; Zakutayev, A.; Major, J. D.; Hao, X.; Walsh, A.; Todorov, T. K.; Saucedo, E. Emerging inorganic solar cell efficiency tables (Version 1). Journal of Physics: Energy **2019**, 1, 032001.
- (10) Wen, X.; Chen, C.; Lu, S.; Li, K.; Kondrotas, R.; Zhao, Y.; Chen, W.; Gao, L.; Wang, C.; Zhang, J.; Niu, G.; Tang, J. Vapor transport deposition of antimony selenide thin film solar cells with 7.6% efficiency. Nature Communications **2018**, 9, 2179.
- (11) Wang, L.; Li, D. B.; Li, K.; Chen, C.; Deng, H. X.; Gao, L.; Zhao, Y.; Jiang, F.; Li, L.; Huang, F.; He, Y.; Song, H.; Niu, G.; Tang, J. Stable 6%-efficient  $\text{Sb}_2\text{Se}_3$  solar cells with a ZnO buffer layer. Nature Energy **2017**, 2, 17046.
- (12) Phillips, L. J.; Savory, C. N.; Hutter, O. S.; Yates, P. J.; Shiel, H.; Mariotti, S.; Bowen, L.; Birkett, M.; Durose, K.; Scanlon, D. O.; Major, J. D. Current enhancement via a  $\text{TiO}_2$  window layer for CSS  $\text{Sb}_2\text{Se}_3$  solar cells: performance limits and high  $V_{oc}$ . IEEE J. Photovoltaics **2019**, 9, 544–551.
- (13) Ding, C.; Zhang, Y.; Liu, F.; Kitabatake, Y.; Hayase, S.; Toyoda, T.; Yoshino, K.; Minemoto, T.; Katayama, K.; Shen, Q. Effect of the conduction band offset on interfacial recombination behavior of the planar perovskite solar cells. Nano Energy **2018**, 53, 17 – 26.
- (14) Kephart, J.; McCamy, J.; Ma, Z.; Ganjoo, A.; Alamgir, F.; Sampath, W. Band alignment of front contact layers for high-efficiency CdTe solar cells. Solar Energy Materials and Solar Cells **2016**, 157, 266 – 275.
- (15) Wallace, S. K.; Butler, K. T.; Hinuma, Y.; Walsh, A. Finding a junction partner for



- candidate solar cell absorbers enargite and bournonite from electronic band and lattice matching. Journal of Applied Physics **2019**, 125, 055703.
- (16) Helander, M.; Greiner, M.; Wang, Z.; Lu, Z. Pitfalls in measuring work function using photoelectron spectroscopy. Applied Surface Science **2010**, 256, 2602 – 2605.
- (17) Schlaf, R.; Murata, H.; Kafafi, Z. Work function measurements on indium tin oxide films. Journal of Electron Spectroscopy and Related Phenomena **2001**, 120, 149 – 154.
- (18) Kraut, S.; Grant, E. A.; Waldrop, J. R.; Kowalczyk, S. P. Precise determination of the valence band edge in x-ray photoemission spectra: application to measurement of semiconductor interface potentials. Physical Review Letters **1980**, 44, 1620–1623.
- (19) King, P. D. C.; Veal, T. D.; Kendrick, C. E.; Bailey, L. R.; Durbin, S. M.; McConville, C. F. InN/GaN valence band offset: High-resolution x-ray photoemission spectroscopy measurements. Phys. Rev. B **2008**, 78, 033308.
- (20) Anderson, R. L. Germanium-Gallium Arsenide Heterojunctions [Letter to the Editor]. IBM Journal of Research and Development **1960**, 4, 283–287.
- (21) Mariotti, S.; Hutter, O. S.; Phillips, L. J.; Yates, P. J.; Kundu, B.; Durose, K. Stability and performance of CsPbI<sub>2</sub>Br thin films and solar cell devices. ACS Applied Materials & Interfaces **2018**, 10, 3750–3760.
- (22) Burton, L. A.; Whittles, T. J.; Hesp, D.; Linhart, W. M.; Skelton, J. M.; Hou, B.; Webster, R. F.; O’Dowd, G.; Reece, C.; Cherns, D.; Fermin, D. J.; Veal, T. D.; Dhanak, V. R.; Walsh, A. Electronic and optical properties of single crystal SnS<sub>2</sub>: an earth-abundant disulfide photocatalyst. J. Mater. Chem. A **2016**, 4, 1312–1318.
- (23) Klein, A. Energy band alignment at interfaces of semiconducting oxides: A review of experimental determination using photoelectron spectroscopy and comparison with theoretical predictions by the electron affinity rule, charge neutrality levels, and the

- common anion rule. Thin Solid Films **2012**, 520, 3721 – 3728, 7th International Symposium on Transparent Oxide Thin Films for Electronics and Optics (TOEO-7).
- (24) Klein, A. Energy band alignment in chalcogenide thin film solar cells from photoelectron spectroscopy. Journal of Physics: Condensed Matter **2015**, 27, 134201.
- (25) Niles, D. W.; Margaritondo, G. Heterojunctions: Definite breakdown of the electron affinity rule. Phys. Rev. B **1986**, 34, 2923–2925.
- (26) Schlaf, R.; Lang, O.; Pettenkofer, C.; Jaegermann, W. Band lineup of layered semiconductor heterointerfaces prepared by van der Waals epitaxy: Charge transfer correction term for the electron affinity rule. Journal of Applied Physics **1999**, 85, 2732–2753.
- (27) Li, D.-B.; Yin, X.; Grice, C. R.; Guan, L.; Song, Z.; Wang, C.; Chen, C.; Li, K.; Cimaroli, A. J.; Awni, R. A.; Zhao, D.; Song, H.; Tang, W.; Yan, Y.; Tang, J. Stable and efficient CdS/Sb<sub>2</sub>Se<sub>3</sub> solar cells prepared by scalable close space sublimation. Nano Energy **2018**, 49, 346 – 353.
- (28) Shiel, H.; Hutter, O. S.; Phillips, L. J.; Turkestani, M. A.; Dhanak, V. R.; Veal, T. D.; Durose, K.; Major, J. D. Chemical etching of Sb<sub>2</sub>Se<sub>3</sub> solar cells: surface chemistry and back contact behaviour. Journal of Physics: Energy **2019**, 1, 045001.
- (29) Tanuma, S.; Powell, C. J.; Penn, D. R. Calculation of electron inelastic mean free paths (IMFPs) VII. Reliability of the TPP-2M IMFP predictive equation. Surface and Interface Analysis **2003**, 35, 268–275.
- (30) Hutter, O. S.; Phillips, L. J.; Yates, P. J.; Major, J. D.; Durose, K. CSS antimony selenide film morphology and high efficiency PV devices. WCPEC-7 Conference Paper **2018**, 0027–0031.
- (31) Dette, C.; Pérez-Osorio, M. A.; Kley, C. S.; Punke, P.; Patrick, C. E.; Jacobson, P.;

- Giustino, F.; Jung, S. J.; Kern, K. TiO<sub>2</sub> Anatase with a Bandgap in the Visible Region. Nano Letters **2014**, 14, 6533–6538.
- (32) Whittles, T. J.; Veal, T. D.; Savory, C. N.; Welch, A. W.; de Souza Lucas, F. W.; Gibbon, J. T.; Birkett, M.; Potter, R. J.; Scanlon, D. O.; Zakutayev, A.; Dhanak, V. R. Core Levels, Band Alignments, and Valence-Band States in CuSbS<sub>2</sub> for Solar Cell Applications. ACS Applied Materials & Interfaces **2017**, 9, 41916–41926.
- (33) Oliva, A.; Solís-Canto, O.; Castro-Rodríguez, R.; Quintana, P. Formation of the band gap energy on CdS thin films growth by two different techniques. Thin Solid Films **2001**, 391, 28 – 35.
- (34) Hobson, T. D. C.; Phillips, L. J.; Hutter, O. S.; Shiel, H.; Swallow, J. E. N.; Savory, C. N.; Nayak, P. K.; Mariotti, S.; Das, B.; Bowen, L.; Jones, L. A. H.; Featherstone, T. J.; Smiles, M. J.; Farnworth, M. A.; Zoppi, G.; Thakur, P. K.; Lee, T.-L.; Snaith, H. J.; Leighton, C.; Scanlon, D. O.; Dhanak, V. R.; Durose, K.; Veal, T. D.; Major, J. D. Isotype Heterojunction Solar Cells Using n-Type Sb<sub>2</sub>Se<sub>3</sub> Thin Films. Chemistry of Materials **2020**, 32, 2621–2630.
- (35) Bechlaghem, S.; Zebentout, B.; Benamara, Z. The major influence of the conduction-band-offset on Zn(O,S)/CuIn<sub>0.7</sub>Ga<sub>0.3</sub>Se<sub>2</sub> solar cells. Results in Physics **2018**, 10, 650–654.
- (36) Pudov, A. O.; Kanevce, A.; Al-Thani, H. A.; Sites, J. R.; Hasoon, F. S. Secondary barriers in CdS-CuIn<sub>1-x</sub>Ga<sub>x</sub>Se<sub>2</sub> solar cells. Journal of Applied Physics **2005**, 97, 064901.
- (37) Prabhakar, R. R.; Moehl, T.; Siol, S.; Suh, J.; Tilley, S. D. Sb<sub>2</sub>S<sub>3</sub>/TiO<sub>2</sub> Heterojunction Photocathodes: Band Alignment and Water Splitting Properties. Chem. Mater. **2020**, <https://doi.org/10.1021/acs.chemmater.0c01581>.
- (38) Mönch, W. Semiconductor Surfaces and Interfaces; Springer, 1993; p 548.

- (39) Miedema, A. R.; de Boer, F. R.; de Chatel, P. F. Empirical description of the role of electronegativity in alloy formation. Journal of Physics F: Metal Physics **1973**, 3, 1558–1576.
- (40) Miedema, A.; de Châtel, P.; de Boer, F. Cohesion in alloys - fundamentals of a semi-empirical model. Physica B+C **1980**, 100, 1 – 28.
- (41) Mönch, W. Electronic Properties of Semiconductor Interfaces; Springer, 1986; p 263.